Cooling, Scattering, and Recombination-The Role of the Material Quality for the Physics of Tin Halide Perovskites

Kahmann, Simon; Shao, Shuyan; Loi, Maria A.

Link to publication in University of Groningen/UMCG research database

Cooling, Scattering, and Recombination—The Role of the Material Quality for the Physics of Tin Halide Perovskites

Simon Kahmann, Shuyan Shao, and Maria A. Loi*

Tin-based perovskites have long remained a side topic in current perovskite optoelectronic research. With the recent efficiency improvement in thin film solar cells and the observation of a long hot carrier cooling time in formamidinium tin iodide ($FASnI_3$), a thorough understanding of the material's photophysics becomes a pressing matter. Since pronounced background doping can easily obscure the actual material properties, it is of paramount importance to understand how different processing conditions affect the observed behavior. Using photoluminescence spectroscopy, thin films of $FASnI_3$ fabricated through different protocols are therefore investigated. It is shown that hot carrier relaxation occurs much faster in highly p-doped films due to carrier–carrier scattering. From high quality thin films, the longitudinal optical phonon energy and the electron–phonon coupling constant are extracted, which are fundamental to understanding carrier cooling. Importantly, high quality films allow for the observation of a previously unreported state of microsecond lifetime at lower energy in $FASnI_3$, that has important consequences for the discussion of long lived emission in the field of metal halide perovskites.

1. Introduction

Metal halide perovskites (HaPs) with a composition of the form ABX_3 (with A being a monovalent cation, B being a divalent metal cation, and X being a monovalent halide anion) are a class of materials with extraordinary properties exploitable in optoelectronic devices. Besides their large absorption coefficients, long charge carrier diffusion lengths, and suitable bandgap energy, it is the possibility to cast thin films from solution that makes them strong candidates for large-scale production of solar cells.[1] Compositional variation furthermore allows for tuning the bandgap of HaPs over a broad part of the visible spectral range into the near infrared region—an important aspect for applications in light emission or multijunction solar cells.[2,3]

Dr. S. Kahmann, Dr. S. Shao, Prof. M. A. Loi
Photophysics and OptoElectronics
Zernike Institute for Advanced Materials
Rijksuniversiteit Groningen
Nijenborgh 4, 9747 AG, Groningen, The Netherlands
E-mail: m.a.loi@rug.nl

The ORCID identification number(s) for the author(s) of this article can be found under https://doi.org/10.1002/adfm.201902963.

A remarkable property of many HaPs that recently moved into the center of attention is the extraordinary long relaxation or cooling time τ_{rel} of charge carriers generated with excess energy above the fundamental bandgap.[4–9] A long relaxation time is one major ingredient necessary for the fabrication of hot carrier solar cells (HCSCs)—devices which offer the possibility for overcoming the Shockley–Queisser limit in single junction solar cells.[10] Interestingly, a very slow hot carrier cooling was recently reported for the tin compound formamidinium tin iodide ($FASnI_3$).[9]

Tin-based perovskites have so far not been studied as extensively as their lead-based counterparts mainly because they tend to degrade quickly upon air exposure.[11] Tin oxidizes from its desired +2 to its +4 form, which causes strong self p-doping of the perovskite. Particularly, the high background hole density is harmful to the solar cell performance due to the significant monomolecular charge recombination loss. Nonetheless, the solar cell community achieved several important improvements in power conversion efficiency (PCE) through the use of special manufacturing protocols, for example, the addition of SnF_2 or $SnCl_2$ as a reducing agent or the introduction of a reducing atmosphere (N_2H_4).[12–15] Similarly, our group showed that the addition of small amounts of 2-phenylethylammonium (PEA) ions on the A-site can stabilize the material, allowing for a better performance in photovoltaic devices.[16]

Given these recent developments, a more thorough understanding of the photophysics of tin perovskites and where it differs/corresponds to the behavior of lead perovskites is necessary. Importantly, the impact of the processing conditions on the optoelectrical behavior has to be understood in order to acquire meaningful insights into the properties intrinsic to tin perovskites.

In this work, we therefore investigate the photophysics of the important formamidinium tin iodide ($FASnI_3$) variant over a range from room temperature down to ≈4 K while carefully changing the film processing conditions. These prototypical samples exhibit striking differences in emission spectra, photoluminescence (PL) lifetimes, and scattering mechanisms—all of which are important to properly classify reported observations on $FASnI_3$ and related materials. Crucially, we are also able to reveal a previously unreported long-lived state in the low temperature phase of $FASnI_3$, which has a lifetime approaching 10 µs.

**ADVANCED
SCIENCE NEWS**

www.advancedsciencenews.com

**ADVANCED
FUNCTIONAL
MATERIALS**

www.afm-journal.de

2. Results and Discussion

We fabricated three sets of samples of $FASnI_3$ thin films (processing details are given in the "Materials and Methods" section in the Supporting Information). Additional to neat $FASnI_3$, these include one with the commonly employed addition of SnF_2 and one with the addition of 0.08 M PEA, as previously introduced by our group.[16] These samples will in the following be indicated as "neat," "SnF_2," and "2D/3D." Especially the latter treatment was shown to increase the film quality, e.g., by ordering the formed crystallites from a random orientation to preferential alignment. Top view scanning electron microscopy (SEM) micrographs, as given in Figure S1 in the Supporting Information, furthermore show the larger crystal size upon SnF_2 addition and the further smoothing of the boundaries for the 2D/3D sample. More details on the effect of these treatments on the film morphology can be found in our previous work.[16] The reduction of self-doping using the latter two protocols, i.e., their higher quality, can be observed readily from the suppression of the Burstein–Moss shift in absorption spectra (Figure S2, Supporting Information).

The effects of these different processing conditions on the photoluminescence at room temperature (RT) are reported in **Figure 1**. The emission peak for the neat film is found at higher energy than for the other two films (1.351 eV vs 1.347 and 1.344 eV for the SnF_2 and 2D/3D films) as shown in Figure 1a. This blue-shift is due to the partial filling of the valence band in neat $FASnI_3$ and was similarly observed before for different concentrations of added SnF_2.[17] Simultaneously, the emission width increases from 99 meV over 107 to 115 meV, which we attribute to increased carrier scattering by both background ions and charge carriers. Moreover, in accordance with earlier reports from our group,[9,16] these spectra also show that despite naming the last sample "2D/3D," the material behaves like the pure 3D variant—the 2D material was shown to merely template the growth of the 3D phase on top.[16] It is important to note that all measurements were carried out under inert atmosphere and the samples were fabricated in a highly clean nitrogen glove box (water and oxygen concentration ≤0.1 ppm). Already brief air exposure can have a very strong effect on the emission characteristics—especially on the low quality neat film (Figure S3, Supporting Information). The 2D/3D sample is much more resilient toward degradation. These strong spectral changes thus underline the importance to know and to control the experimental parameters for meaningful conclusions about this material.

The position and shape of the spectra furthermore depends strongly on the excitation conditions. As shown in Figure S4 in the Supporting Information, the emission peak shifts toward higher energy upon increasing the fluence of the exciting laser. This is due to a combination of both state filling and hot carrier PL.[9] Nonetheless, this only becomes dominant when exceeding several hundred nJ cm^{-2}. We thus study our samples in the region of low-level excitation, unless stated otherwise. The power dependence in Figure 1b shows that in this regime, the samples' integrated emission scales linearly with the excitation fluence, indicating the PL to be due to monomolecular processes. Since we do not observe any evidence for exciton formation, we attribute this behavior to a significant amount of
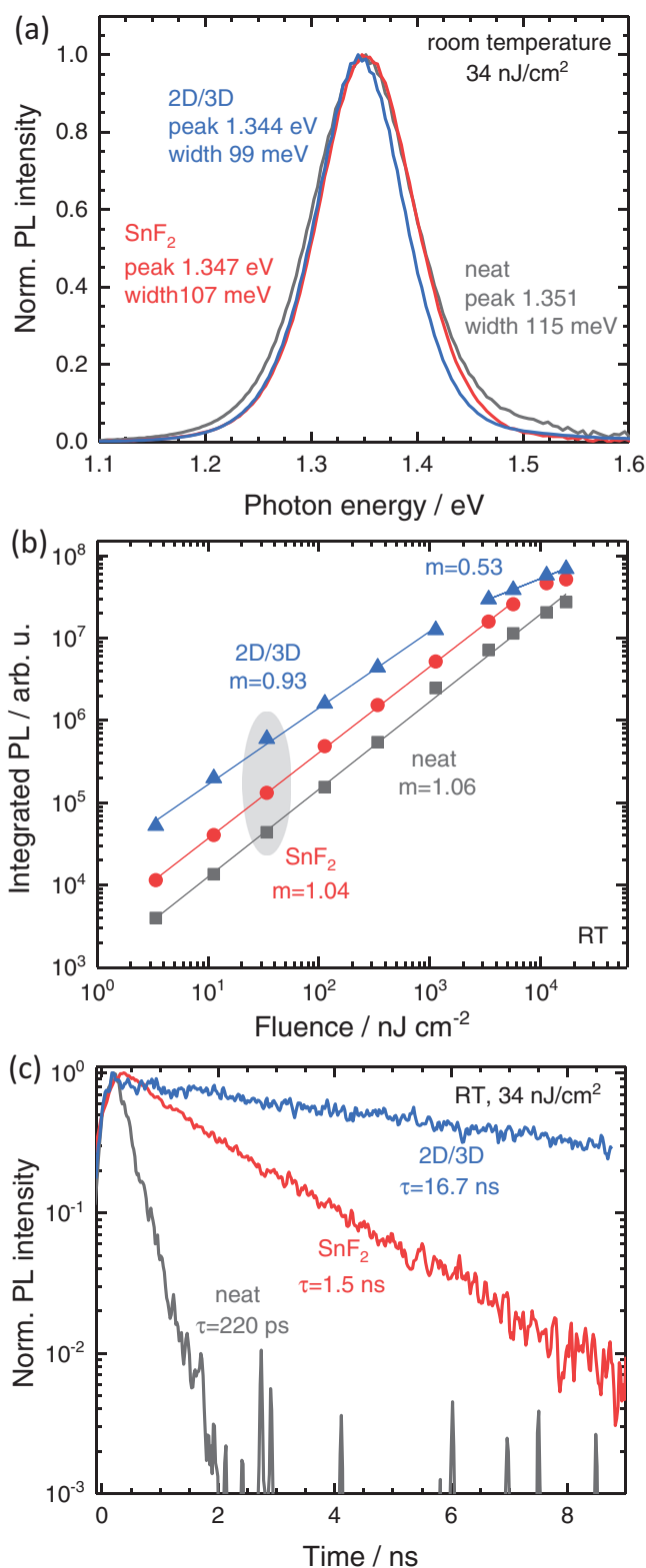
Figure 1. The room temperature PL indicates the superior quality of SnF_2 and 2D/3D $FASnI_3$. a) This is observable by the blue-shifted and broadened emission of neat $FASnI_3$ due to its higher doping. b) The integrated PL is highest for the 2D/3D material, and c) the PL lifetime is longest. b) Nonetheless, all investigated samples exhibit a linear increase with the excitation fluence in the low intensity regime, indicating monomolecular recombination.

background holes to be present even in the high quality 2D/3D film, which is supported by the positive Seebeck coefficient and high conductivity of the 2D/3D film.[16]

Figure 1c, finally, displays the time resolved band edge emission under low excitation. Analogous to the general discussion outlined above, we again find a strong impact of the processing conditions leading to a fast decay for the neat film and to longer lifetimes for the films processed with additives. While the PL decays monoexponentially in all cases, the extracted lifetimes range from 220 ps to 16.7 ns, i.e., vary by about two orders of magnitude just due to different casting protocols. We would like to underline that transient PL measurements thus serve as a much stronger indicator for the film quality than steady state measurements. Importantly, the obtained kinetics are independent of the excitation fluence and reproducible in the low-excitation regime (Figure S5, Supporting Information).

One of the most intriguing aspects of $FASnI_3$ is the extended hot carrier lifetime. As we discussed in an earlier report, the loss of the hot carriers' excess energy can involve many different steps.[10] The first stage after excitation is governed by rapid carrier–carrier scattering, or thermalization, which is then followed by the interaction of hot carriers with the lattice through

phonons. For the lead-based variants, the field's consensus is that this initial interaction is predominantly due to the emission of longitudinal optical (LO) phonons, i.e., through the so-called Fröhlich interaction.

We use this report to underline an important aspect for the investigation of hot charge carriers in tin perovskites. **Figure 2** reports the time resolved PL spectra at different delays for the extreme cases of neat $FASnI_3$ and the 2D/3D sample. Under the high excitation, band filling and hot carriers lead to the aforementioned blue-shift of the emission. The emission profiles show that the time-dependent red-shift of the emission still occurs after 1000 ps in case of the 2D/3D sample in Figure 2c. The neat film (Figure 2d), in contrast, does not exhibit any spectral changes after 200 ps and thereby shows the corrupted hot carrier cooling time in this sample. Their drastically shorter hot carrier lifetime is presumably due to the increased loss of excess energy to cold charge carriers during the initial scattering phase. This important aspect underlines how poor film quality will inevitably lead to wrong conclusions about the photophysics in this material.

A powerful way to investigate the electron–phonon interaction is via temperature dependent photoluminescence spectroscopy.
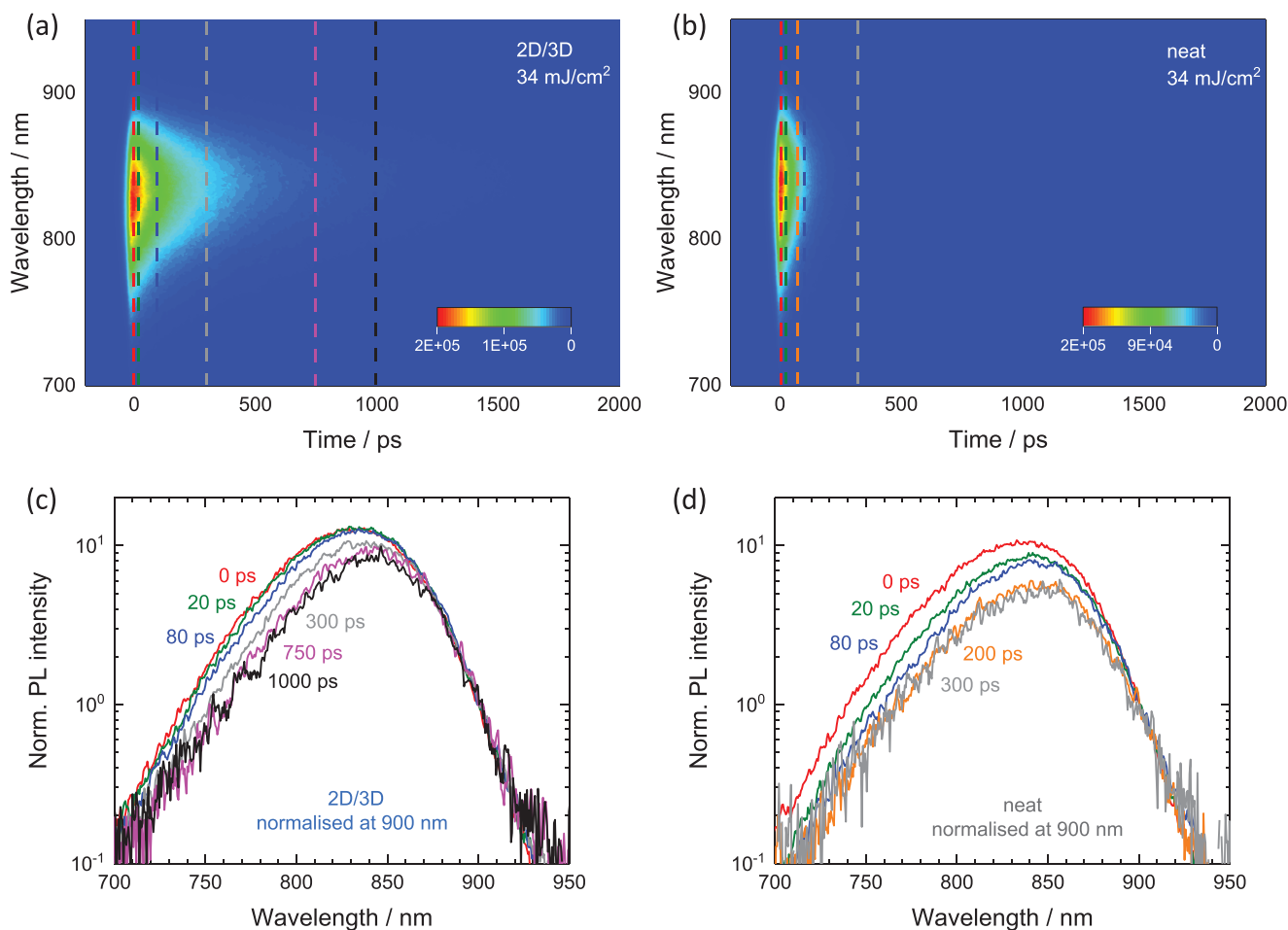

Figure 2. Streak camera plots for a) 2D/3D and b) neat $FASnI_3$ under high excitation. The vertical lines indicate the extracted spectra given in (c) and (d). The data in (c) and (d) were normalized at 900 nm to show the evolution of the spectral shape. The carrier cooling in the neat film is complete after 200 ps.
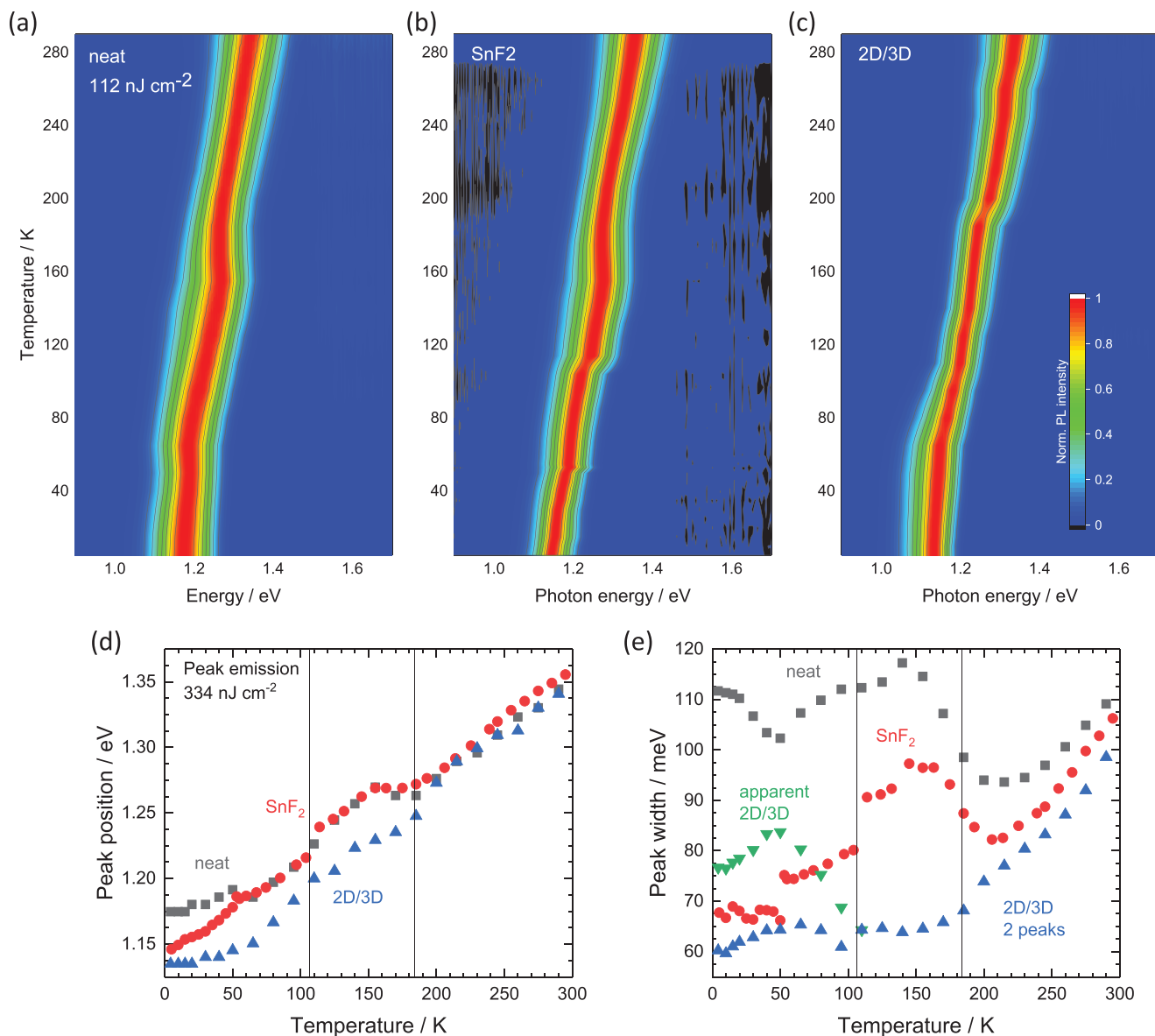
**ADVANCED
SCIENCE NEWS**

www.advancedsciencenews.com

**ADVANCED
FUNCTIONAL
MATERIALS**

www.afm-journal.de

Figure 3. Normalized temperature dependent PL spectra of a) the neat, b) the SnF$_2$, and c) the 2D/3D sample. d) All materials exhibit a gradual red-shift of the peak upon lowering the temperature, but e) the linewidth behaves drastically different. At around 180 and 110 K (possibly also at 50 K), a discontinuity indicates a phase transition (consider vertical lines in (d)). The peak width of the higher quality samples decreases with temperature, but broadens again in the low temperature phase for the 2D/3D variant (green symbols). Fitting this signal with two peaks leads to a width indicated by the blue symbols.

This technique has consequently been used to determine the LO phonon energy E_{LO} and the electron–phonon coupling strength γ_{LO} for a variety of perovskite compositions in thin films, quantum dots, and single crystals.[18–22] Such studies have the additional benefit of revealing a plethora of useful information about the material properties, such as possible phase transitions, the nature of emitting species (singlets, triples, free carriers), and the impact of temperature on the bandgap energy E_{gap}.

In this spirit, we present the temperature dependent steady state emission for all three samples (normalized for each spectrum), given in **Figure 3**a–c (absolute spectra in Figure S6, Supporting Information). All FASnI$_3$ films exhibit a significantly broader emission than previously observed for

FAPbI$_3$.[18,19] At 4 K, the linewidths reduce to 70–110 meV (consider Figure S7 in the Supporting Information) as opposed to ≈20 meV for FAPbI$_3$. As detailed in Figure 3d, all samples exhibit the previously observed blue-shift of the emission peak with increasing temperature.[9,17,23] Although most materials show the inverse trend, this is the common behavior for HaPs and was similarly observed for example in lead chalcogenides.[24] The explanation for this anomalous trend is currently under discussion. While Saran et al.,[25] for example, use a Bose–Einstein two-oscillator model to explain this behavior, Kontos et al. invoke the off-centering (emphanisis) of the metal ions in the MeI$_6$ octahedra as well as additional dynamic symmetry breaking to explain this trend.

Tracking the peak position reveals a discontinuity at ≈180 K and 110 K (possibly also around 50 K). This suggests that FASnI$_3$ forms three (four) different crystal phases over the investigated temperature range. Stoumpos et al. determined the RT phase to be orthorhombic with *Amm*2 symmetry and below 180 K to be orthorhombic with *Imm*2 symmetry, i.e., distorted octahedra.[26] To the best of our knowledge, data on the low temperature phase is not available at this moment. Interestingly, both the neat films and the SnF$_2$ sample show a significantly higher peak energy in the intermediate phase than the 2D/3D film. The strong blue-shift of the latter's emission around 180 K (when increasing *T*) is also not found for those two films—in contrast, the peak energy slightly red-shifts—an aspect to which we shall return below.

Examining the PL linewidth allows for drawing conclusions about the dominant scattering mechanisms for charge carriers.[27] The respective data in Figure 3e displays large differences in this behavior. In the high temperature phase, the linewidth decreases for all three samples when lowering the temperature. Toward the phase transition at 180 K, however, the neat and SnF$_2$ sample exhibit a distinct widening while the 2D/3D sample reaches a minimum of around 65 meV. Note how these different trends are analogous to the trends for the peak positions discussed above. As reported in our earlier work, the 2D/3D sample can be thought of as a highly ordered 3D film templated onto a 2D interface layer on the substrate.[16] We thus speculate that this templating suppresses phase inhomogeneities occurring due to the reorientations below 180 K.

In the low temperature phase below 110 K, finally, all samples give rise to different trends. The neat film exhibits small changes around a linewidth of 110 meV, largely independent of the temperature. In contrast, the SnF$_2$ sample shows a strong reduction of the linewidth around 110 K, which further decreases to ≈70 meV below 50 K. The 2D/3D sample shows an unexpected and pronounced broadening of the emission (from 65 meV at 110 K to 83 meV at 50 K; indicated in Figure 3e green as "apparent 2D/3D"). As we shall discuss further below, this is due to the appearance of a second emitting state, which is evident from the time dependent PL in **Figure 4** (also consider Figure S6e in the Supporting Information). Peak deconvolution gives rise to the blue symbols in Figure 3e, which show that the 2D/3D sample actually exhibits a narrower line of around 60 meV at 4 K.

Generally, the linewidth ΔE is the sum of an inhomogeneous background term (Γ_{inh}), for example, due to disorder or doping, plus a scattering term due to acoustic (Γ_A) and optical phonons (Γ_{LO}), and an impurity term (Γ_{imp}), leading to $\Delta E = \Gamma_{inh} + \Gamma_A + \Gamma_{LO} + \Gamma_{imp}$. Given the large and virtually constant linewidth below ≈150 K, we follow Wright et al.'s approach[19] and assume the width to only depend on the inhomogeneous term and optical phonon scattering, i.e., $\Delta E = \Gamma_{inh} + \Gamma_{LO} = \Gamma_{inh} + \frac{\gamma_{LO}}{e^{E_{LO}/k_BT}-1}$ (where γ_{LO} is the electron–optical phonon coupling constant and E_{LO} is the optical phonon energy). The fitted curve is given in Figure S8 in the Supporting Information. The extracted LO phonon energy of 68 meK is significantly larger than for FAPbI$_3$, which lies around 15 meV.[18,19] Similarly, the coupling constant of 511 meK is a surprising order of magnitude larger than for lead iodide variants or MASnI$_3$[22] and even exceeds the 161.9 and 226 meV reported for MAPbBr$_3$ or Cs$_2$AgBiBr$_6$.[20,21]
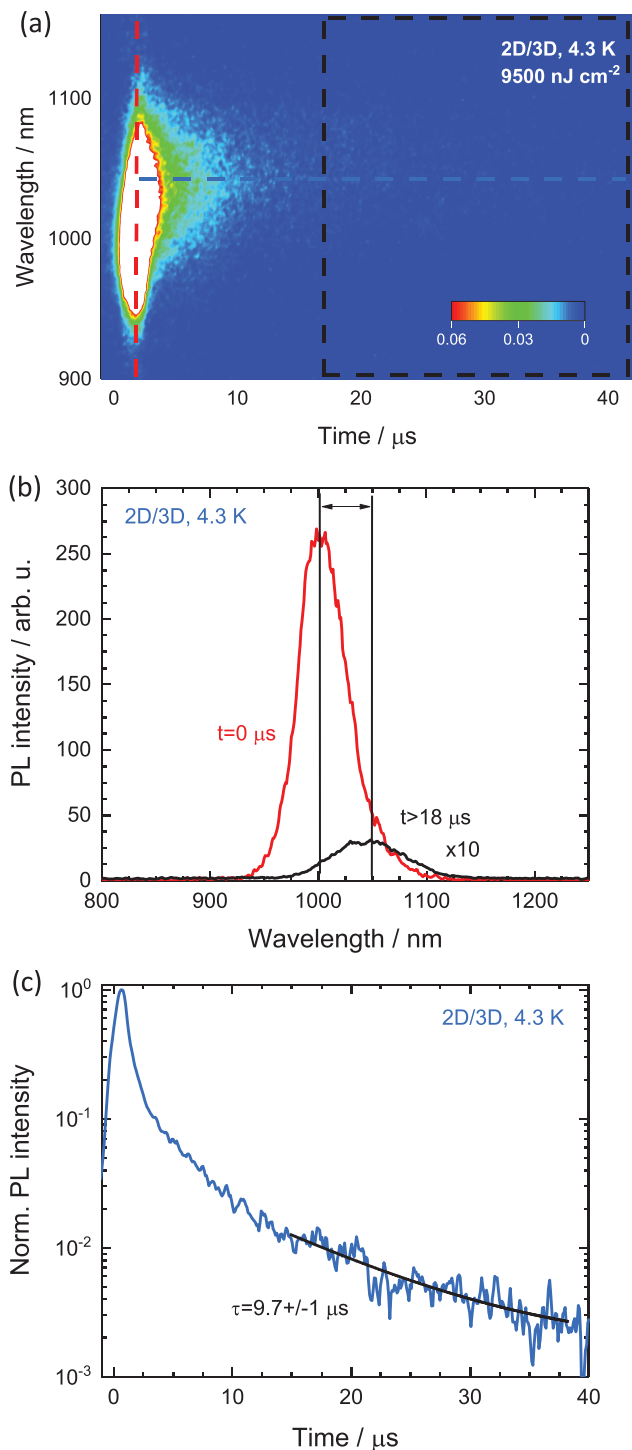

Figure 4. a) The streak camera plot of 2D/3D FASnI$_3$ at 4.3 K reveals a long-lived component at low energy. The normalized intensity above 0.06 is clipped for better visibility. b) Extracting the initial spectrum and the long-lived emission shows the different maxima (≈1000 vs 1050 nm) at the different time scales. c) The transient at 1050 nm gives a lifetime approaching 10 µs, at long delay.

As additional evidence to show that ordering and doping are the major source for the linewidth variation, we measured the SnF$_2$ sample again after aging. The spectra are given in

**ADVANCED
SCIENCE NEWS**

www.advancedsciencenews.com

**ADVANCED
FUNCTIONAL
MATERIALS**

www.afm-journal.de

Figures S9 and S10 in the Supporting Information, showing the drastic changes in the emission behavior. Unlike the data in Figure 3b, the spectra are uniformly broad over the entire temperature range, showing that tin oxidation is the dominant source of the spectral changes.

Time resolved studies confirm the presence of the second state at low temperature. The normalized streak camera plot of the 2D/3D sample in Figure 4a shows that most of the emission decays within the first 2 µs (intensity above 6% is clipped). Additionally, though, there is a pronounced emission tail still decaying at the end of the measurement window of 42 µs. As given in Figure 4b, this latter emission is centered around 1050 nm (1.18 eV), as opposed to the initial 1000 nm (1.24 eV) (unaccounted for camera sensitivity). The peak energy is larger than what might be expected from Figure 3, since a much higher fluence needs to be employed in order to obtain a measurable long-lived signal (intensity dependent spectra are given in Figure S11, Supporting Information). The extracted lifetime of the long-lived component amounts to ≈9.7 µs (Figure 4c). This order of magnitude additionally indicates a different origin than for the emission at early times. Since the SnF_2 sample (data given in Figure S12, Supporting Information) clearly shows its presence as well, we rule out that this effect is an artifact from the 2D components in the film. Given that this low energy emission is more pronounced for the high quality films, we furthermore exclude it to be due to a trap to band transition.[22]

It is worthwhile to closely examine the emergence of this long-lived signal as a function of temperature. If this emission were purely due to the lower thermal energy of carriers at low temperature, one would expect a gradual increase of this low energy signal when decreasing the temperature. In contrast, as suggested by Figure 3c, the signal appears abruptly at the transition to the low temperature phase around 110 K. We thus measured the transient PL also for different temperatures (see streak plots in Figure S13 in the Supporting Information). For four different measurements, taken at 4.3, 50, 110, and 180 K, the behavior of the former two are almost identical with a pronounced long-lived component still visible after 8 µs (**Figure 5**a). At 110 K, however, the emission is virtually finished after 2 µs and the one at 180 K occurs even faster (resolution limited). Importantly, as can be seen from the plots in Figure S13 in the Supporting Information, the small long-lived contribution at 110 K is due to the main peak and not shifted to lower energy.

The PL on a shorter time scale up to 10 ns is given in Figure 5. Again, the behavior is markedly different for the two temperature ranges. While the decay is monoexponential ($\tau \approx 20$ ns) at room temperature and can best be described with a stretched exponential at intermediate temperatures, the intensity clearly decreases biexponentially at low temperature. For 4.3 and 50 K, the transients are virtually identical with a slow component of $\tau_2 \approx 50$ ns and a fast one, τ_1, below 1 ns (resolution limited). We propose that this fast component is due to the transition toward the lower lying state and therefore vanishes in the higher temperature phase. The stark contrast of τ around the phase transition and the different impact of temperature variation within the phases (constant τ at low T and increasing τ in the higher temperature phases) also suggest a strong impact of the crystal structure on the nature of
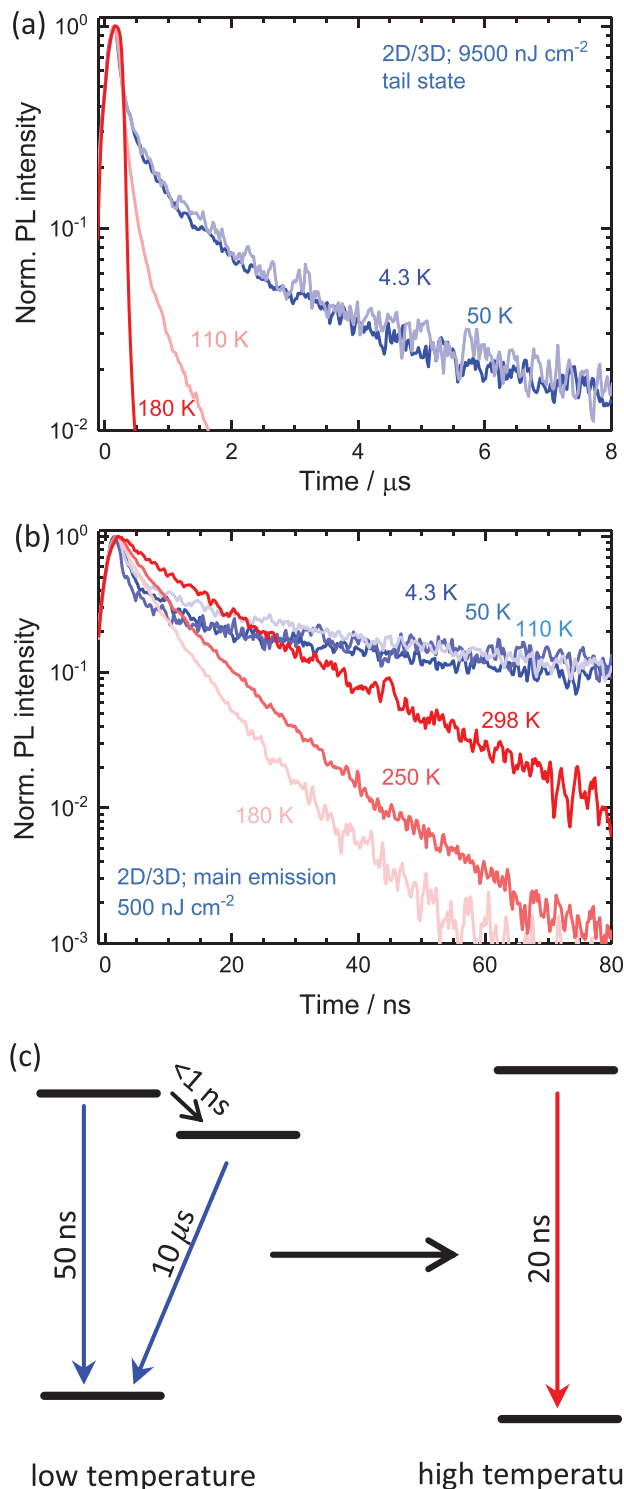

Figure 5. Temperature dependence of the transient PL of 2D/3D $FASnI_3$ at a) long (µs) and b) short (ns) delay times. The former shows that the long-lived tail of the PL vanishes in the higher temperature phases. Simultaneously, (b) shows a clear biexponential behavior at low temperature (fast component <1 ns; slow component ≈50 ns), which switches to a fast, almost monoexponential, behavior at 110 K. Upon further increasing the temperature, the decay slows down, giving a lifetime approaching 20 ns at room temperature. c) We propose an energy scheme involving two emitting states in the low temperature phase, which changes into a one-state model above 110 K.

1902963 (6 of 8)

the transition. Importantly, we observe these general trends also for the neat film (Figure S14, Supporting Information) and can thus exclude any of these effects to be solely due to the 2D templating.

The emergence of a long-lived emission tail at lower energy has been observed before in lead-based perovskites, but to our knowledge, we are the first to report its presence in a purely tin-based composition. Explanations for this phenomenon in Pb compounds include a slightly indirect bandgap, possibly due to Rashba splitting,[28–30] a bound exciton, possibly with triplet character[18] or the presence of both ordered and disordered domains at low T.[31] We rule out the latter based on the above argument that order in the 2D/3D sample is increased. Further studies on the origin of this transition will have to include detailed calculations on the material's crystal structure and further studies on highly ordered samples—ideally on single crystals. Since tin atoms are much lighter ($Z = 50$) than lead atoms ($Z = 82$), whose spin–orbit coupling is often invoked to motivate the strong Rashba–Dresselhaus effect,[32–34] the mere presence of an emission tail in $FASnI_3$ is already a discovery that offers important insights into the properties of this material class.

3. Conclusion

In conclusion, we investigated the photophysics of $FASnI_3$ thin films of different quality deposited via different protocols. For neat $FASnI_3$, we observe that the PL and absorption characteristics are generally governed by the high doping concentration due to the easy oxidation of tin. The use of SnF_2 as reducing agent or additional templating of $FASnI_3$ through the use of a thin layer of 2D perovskite is necessary for studying the real material properties including PL peak position, linewidth and lifetime, as well as the recently reported long cooling time of hot charge carriers.

As an important discovery, we observe a long-lived emission tail at an energy below the main peak when the material is cooled down beyond the phase transition around 110 K. This change is accompanied by the emergence of a short decay component of the main emission, which we interpret as being due to the transition of carriers from the high to the low energy state. The lifetime of the latter is $\approx$10 µs, suggesting its origin to be either due to triplet emission or a slightly indirect bandgap. The latter is often attributed to Rashba splitting in lead-based perovskites, in which heavy Pb ions exhibit a strong spin–orbit coupling. The observation of such a feature in a tin compound of relatively lower atomic number has important consequences for the understanding of this material class.

Having thus demonstrated the great impact of the film quality on the photophysical behavior of $FASnI_3$, we propose that further studies should ideally focus on single crystals to ascertain intrinsic material conditions.

Supporting Information

Supporting Information is available from the Wiley Online Library or from the author.

[1] M. A. Green, A. Ho-Baillie, H. J. Snaith, *Nat. Photonics* **2014**, *8*, 506.
[2] D. P. McMeekin, G. Sadoughi, W. Rehman, G. E. Eperon, M. Saliba, M. T. Horantner, A. Haghighirad, N. Sakai, L. Korte, B. Rech, M. B. Johnston, L. M. Herz, H. J. Snaith, *Science* **2016**, *351*, 151.
[3] L. Protesescu, S. Yakunin, M. I. Bodnarchuk, F. Krieg, R. Caputo, C. H. Hendon, R. X. Yang, A. Walsh, M. V. Kovalenko, *Nano Lett.* **2015**, *15*, 3692.
[4] G. Xing, N. Mathews, S. Sun, S. S. Lim, Y. M. Lam, M. Grätzel, S. Mhaisalkar, T. C. Sum, *Science* **2013**, *342*, 344.
[5] O. Flender, J. R. Klein, T. Lenzer, K. Oum, *Phys. Chem. Chem. Phys.* **2015**, *17*, 19238.
[6] X. Deng, X. Wen, S. Huang, R. Sheng, T. Harada, T. W. Kee, M. Green, A. Ho-Baillie, *J. Phys. Chem. C* **2016**, *120*, 2542.
[7] J. Yang, X. Wen, H. Xia, R. Sheng, Q. Ma, J. Kim, P. Tapping, T. Harada, T. W. Kee, F. Huang, Y.-B. Cheng, M. Green, A. Ho-Baillie, S. Huang, S. Shrestha, R. Patterson, G. Conibeer, *Nat. Commun.* **2017**, *8*, 14120.
[8] D. Niesner, H. Zhu, K. Miyata, P. P. Joshi, T. J. S. Evans, B. J. Kudisch, M. T. Trinh, M. Marks, X.-Y. Zhu, *J. Am. Chem. Soc.* **2016**, *138*, 15717.
[9] H.-H. Fang, S. Adjokatse, S. Shao, J. Even, M. A. Loi, *Nat. Commun.* **2018**, *9*, 243.
[10] S. Kahmann, M. A. Loi, *J. Mater. Chem. C* **2019**, *7*, 2471.
[11] S. Adjokatse, S. Kahmann, H. Duim, M. A. Loi, *APL Mater.* **2019**, *7*, 031116.
[12] M. H. Kumar, S. Dharani, W. L. Leong, P. P. Boix, R. R. Prabhakar, T. Baikie, C. Shi, H. Ding, R. Ramesh, M. Asta, M. Graetzel, S. G. Mhaisalkar, N. Mathews, *Adv. Mater.* **2014**, *26*, 7122.
[13] W. Liao, D. Zhao, Y. Yu, C. R. Grice, C. Wang, A. J. Cimaroli, P. Schulz, W. Meng, K. Zhu, R. G. Xiong, Y. Yan, *Adv. Mater.* **2016**, *28*, 9333.
[14] K. P. Marshall, M. Walker, R. I. Walton, R. A. Hatton, *Nat. Energy* **2016**, *1*, 16178.
[15] T.-B. Song, T. Yokoyama, C. C. Stoumpos, J. Logsdon, D. H. Cao, M. R. Wasielewski, S. Aramaki, M. G. Kanatzidis, *J. Am. Chem. Soc.* **2017**, *139*, 836.
[16] S. Shao, J. Liu, G. Portale, H.-H. Fang, G. R. Blake, G. H. ten Brink, L. J. A. Koster, M. A. Loi, *Adv. Energy Mater.* **2018**, *8*, 1702019.
[17] R. L. Milot, M. T. Klug, C. L. Davies, Z. Wang, H. Kraus, H. J. Snaith, M. B. Johnston, L. M. Herz, *Adv. Mater.* **2018**, *30*, 1804506.

[18] H.-h. Fang, F. Wang, S. Adjokatse, N. Zhao, J. Even, M. Antonietta Loi, *Light: Sci. Appl.* **2016**, *5*, e16056.

[19] A. D. Wright, C. Verdi, R. L. Milot, G. E. Eperon, M. A. Pérez-Osorio, H. J. Snaith, F. Giustino, M. B. Johnston, L. M. Herz, *Nat. Commun.* **2016**, *7*, 11755.

[20] H. C. Woo, J. W. Choi, J. Shin, S.-H. Chin, M. H. Ann, C.-L. Lee, *J. Phys. Chem. Lett.* **2018**, *9*, 4066.

[21] J. A. Steele, P. Puech, M. Keshavarz, R. Yang, S. Banerjee, E. Debroye, C. W. Kim, H. Yuan, N. H. Heo, J. Vanacken, A. Walsh, J. Hofkens, M. B. J. Roeffaers, *ACS Nano* **2018**, *12*, 8081.

[22] T. Handa, T. Aharen, A. Wakamiya, Y. Kanemitsu, *Phys. Rev. Mater.* **2018**, *2*, 075402.

[23] E. S. Parrott, T. Green, R. L. Milot, M. B. Johnston, H. J. Snaith, L. M. Herz, *Adv. Funct. Mater.* **2018**, *28*, 1802803.

[24] M. Grundmann, *The Physics of Semiconductors*, Graduate Texts in Physics, Springer, Berlin **2010**.

[25] R. Saran, A. Heuer-Jungemann, A. G. Kanaras, R. J. Curry, *Adv. Opt. Mater.* **2017**, *5*, 1700231.

[26] C. C. Stoumpos, C. D. Malliakas, M. G. Kanatzidis, *Inorg. Chem.* **2013**, *52*, 9019.

[27] G. Morello, M. De Giorgi, S. Kudera, L. Manna, R. Cingolani, M. Anni, *J. Phys. Chem. C* **2007**, *111*, 5846.

[28] T. Wang, B. Daiber, J. M. Frost, S. A. Mann, E. C. Garnett, A. Walsh, B. Ehrler, *Energy Environ. Sci.* **2017**, *10*, 509.

[29] D. Niesner, M. Hauck, S. Shrestha, I. Levchuk, G. J. Matt, A. Osvet, M. Batentschuk, C. Brabec, H. B. Weber, T. Fauster, *Proc. Natl. Acad. Sci. USA* **2018**, *115*, 9509.

[30] B. Wu, H. Yuan, Q. Xu, J. A. Steele, D. Giovanni, P. Puech, J. Fu, Y. F. Ng, N. F. Jamaludin, A. Solanki, S. Mhaisalkar, N. Mathews, M. B. J. Roeffaers, M. Grätzel, J. Hofkens, T. C. Sum, *Nat. Commun.* **2019**, *10*, 484.

[31] M. I. Dar, G. Jacopin, S. Meloni, A. Mattoni, N. Arora, A. Boziki, S. M. Zakeeruddin, U. Rothlisberger, M. Grätzel, *Sci. Adv.* **2016**, *2*, e1601156.

[32] J. Even, L. Pedesseau, J.-m. Jancu, C. Katan, *J. Phys. Chem. Lett.* **2013**, *4*, 2999.

[33] A. Stroppa, D. Di Sante, P. Barone, M. Bokdam, G. Kresse, C. Franchini, M.-H. Whangbo, S. Picozzi, *Nat. Commun.* **2014**, *5*, 5900.

[34] S. McKechnie, J. M. Frost, D. Pashov, P. Azarhoosh, A. Walsh, M. van Schilfgaarde, *Phys. Rev. B* **2018**, *98*, 085108.